Vibronic structure of alkoxy radicals via photoelectron spectroscopy

Tanya M. Ramond, Gustavo E. Davico, Rebecca L. Schwartz, and W. Carl Lineberger
JILA, University of Colorado and National Institute for Standards and Technology, and Department of Chemistry and Biochemistry, University of Colorado, Boulder, Colorado 80309-0440

(Received 12 August 1999; accepted 19 October 1999)

Ultraviolet photoelectron spectra of CH_3O^-, $CH_3CH_2O^-$, $(CH_3)_2CHO^-$, $(CH_3)_3CO^-$, as well as CD_3O^- and $CD_3CD_2O^-$ are presented, providing improved electron affinities and new information on vibronic coupling in the corresponding neutral radicals. Jahn-Teller vibronic transitions are assigned to *e* vibrational modes of $\tilde{X}\,^2E$ CH_3O. The excitation energy of the $\tilde{A}\,^2A'$ state of CH_3CH_2O with respect to the $\tilde{X}\,^2A''$ state is observed directly at 355 ± 10 cm^{-1}. Vibronic coupling between these low-lying electronic states perturbs the observed vibronic levels. Features of the $(CH_3)_2CHO^-$ photoelectron spectrum are assigned. The splitting between the $\tilde{X}\,^2A'$ and $\tilde{A}\,^2A''$ states of $(CH_3)_2CHO$ is determined to be 1225 ± 65 cm^{-1}. Significant vibronic coupling is not observed in $(CH_3)_2CHO$. Vibrational assignments are made for the spectral features of $(CH_3)_3CO$ and no Jahn-Teller effects are observed directly. Electron affinities (EAs) for the neutrals (RO) are (in eV); $EA(CH_3O)=1.572\pm0.004$; $EA(CD_3O)=1.559\pm0.004$; $EA(CH_3CH_2O)=1.712\pm0.004$; $EA(CD_3CD_2O)=1.699\pm0.004$; $EA((CH_3)_2CHO)=1.847\pm0.004$; $EA((CH_3)_3CO)=1.909\pm0.004$. Bond dissociation energies of ROH, D_{300}(RO–H), along with $\Delta_f H_{300}$(RO), $\Delta_f H_{300}(RO^-)$, and $\Delta_f H_{300}(RO^+)$ are derived. © *2000 American Institute of Physics.* [S0021-9606(00)00303-2]

I. INTRODUCTION

There is great motivation to understand the structure and properties of alkoxides due to their prevalence in combustion processes, interstellar and atmospheric chemistry, and as intermediaries in hydrocarbon reactions. However, the theoretical challenges posed by their inherent structure also offer great motivation for their investigation.

Methoxy radical in particular is one of the smallest organics, which makes it well-suited to study via both experiment and calculation. Consequently, there has been no shortage of experimental work on this ubiquitous radical. Some of the earlier research involved laser magnetic resonance (LMR),[1] microwave studies,[2] and negative ion photoelectron spectroscopy,[3] as well as numerous fluorescence spectroscopic examinations of the $\tilde{A}$–$\tilde{X}$ electronic transitions;[4–9] however, analysis of much of this data was complicated by the overlap and congestion due to room temperature samples as well as poor resolution. Furthermore, there was no indication of any Jahn-Teller effects that would be expected as a result of both the electronic degeneracy of the ^2E ground state and the high-symmetry C_{3v} configuration. Supersonic expansion of the sample in laser-induced fluorescence (LIF) experiments significantly clarified the spectral features,[10–14] permitting the first direct observation of Jahn-Teller activity in methoxy radical.[15] However, it was only within the past several years that the advent of improved resolution techniques in conjunction with supersonic expansions allowed the biggest step toward understanding the spectroscopy of methoxy radical.[16,17] Specifically, the rotationally resolved stimulated emission pumping (SEP) studies have allowed assignment of vibronic symmetry to the CH_3O spectroscopic features because the rotational profile of a transition is a signature of the vibronic symmetry of the states involved.[18,19]

Such information has been a breakthrough for advancing the theoretical understanding of CH_3O and its Jahn-Teller activity. Early theoretical works have computed geometries,[20,21] and Jahn-Teller stabilization energies and distortions.[22] It is only recently that full treatments with the ability to predict spectroscopic features have started to appear.[23] Specifically, in a recent review, Barckholtz and Miller[24] presented the first theoretical treatment of the Jahn-Teller problem including a multimode analysis of both linear and quadratic Jahn-Teller coupling as well as spin–orbit coupling. They were able to incorporate Temps' rotationally resolved SEP data into their model, which in turn calculated the Jahn-Teller parameters that fully characterize the Jahn-Teller activity of the radical.

There have been considerably fewer studies involving CH_3CH_2O, $(CH_3)_2CHO$, and $(CH_3)_3CO$. Negative ion photoelectron spectra of the anions have established electron affinities (EAs) for these three species, although the resolution of the spectra were not sufficient to yield significant spectral detail.[25,26] Like CH_3O, the majority of the investigations of CH_3CH_2O have employed fluorescence spectroscopy.[5,9,10,27–29] Most recently, LIF of jet-cooled CH_3CH_2O has allowed spectroscopic identification of several vibrational modes.[30] Various *ab initio* calculations have been performed on CH_3CH_2O (Refs. 31,32) and $CH_3CH_2O^-$;[20] however, there appears to be some discrepancy as to the symmetry of the ground electronic state of the radical.[25,27,29] Fluorescence excitation spectra of $(CH_3)_2CHO$ were re-

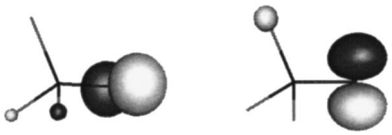

FIG. 1. Schematic of the two degenerate highest occupied molecular orbitals of $\tilde{X}\,^1A_1$ CH_3O^-.

corded to determine rate constants for reaction with various gases.[5,33] In addition, Foster *et al.*[10] obtained rotationally resolved spectra for jet-cooled CH_3O, CH_3CH_2O, as well as $(CH_3)_2CHO$. Based on the rotational structure of the spectra, they assign the ground state of ethoxy radical to be $^2A''$ with a low-lying $^2A'$ state, whereas in iso-propoxy radical, the rotational signature of the fluorescence transitions suggests that the symmetry switches to a $^2A'$ ground state with a $^2A''$ first excited state. Aside from the EA determination in the PES study,[25] our understanding of tert-butoxy extends to a structure calculation of the anion and radical[6,20] and measurement of the electron photodetachment cross section of the anion.[6]

The suite of alkoxides chosen in this work is of particular interest as a study of substitution effects. Methoxide is a closed-shell anion with C_{3v} symmetry. The highest occupied molecular orbitals involve the two nonbonding essentially atomic p orbitals highly localized on the oxygen atom.[11,15,21,22] The 3.408 eV laser photon can photodetach an electron from either the p_x or the p_y orbital, resulting in two energetically equivalent configurations for the radical. A schematic of these degenerate orbitals is shown in Fig. 1. The degenerate electronic state coupled with the C_{3v} symmetry of the radical causes a Jahn-Teller effect in CH_3O. Replacing one of the hydrogens in CH_3O with a methyl group to yield CH_3CH_2O breaks the C_{3v} of CH_3O. This should only be a small perturbation away from the C_{3v} configuration, and thus the resultant splitting in energy of the previously degenerate p-like orbitals is expected to be small. Substituting two hydrogens in CH_3O for methyl groups gives $(CH_3)_2CHO$. This can be thought of as an even larger departure than in CH_3CH_2O away from the methoxy radical C_{3v} structure and thus perturbing the orbital energies even further. However, if we replace each hydrogen in CH_3O with a methyl group to obtain $(CH_3)_3CO$, we return to the C_{3v} symmetry of CH_3O and accordingly we would expect Jahn-Teller effects to be manifested in this radical. In this paper we attempt to characterize these highest occupied molecular orbitals and their interactions via the $\tilde{X}\leftarrow\tilde{X}$ and $\tilde{A}\leftarrow\tilde{X}$ photoelectron spectra as the number of methyl groups substituted for hydrogens increases. We present anion photoelectron spectra of the alkoxides CH_3O^-, $CH_3CH_2O^-$, $(CH_3)_2CHO^-$, and $(CH_3)_3CO^-$, as well as CD_3O^- and $CD_3CD_2O^-$ using a photon energy of 3.408 eV for different laser polarization angles and different sample temperatures. In addition, *ab initio* calculations for ethoxy and iso-propoxy anions and radicals are presented in order to guide the assignment of the spectral peaks.

II. EXPERIMENT

As the experimental technique has been presented previously in great detail,[34] only a synopsis of the negative ion photoelectron spectrometer is given here. Ions are synthesized in a flowing afterglow apparatus operating under approximately 0.5 Torr of pressure from a helium buffer gas. Oxygen anion (O^-) is produced by seeding O_2 through a microwave discharge, and it then reacts with methane to produce hydroxide anion. Proton abstraction from the corresponding alcohol by hydroxide anion yields the desired alkoxide anion as outlined in the following reactions:

$$O^- + CH_4 \rightarrow OH^- + CH_3, \tag{1}$$

$$ROH + OH^- \rightarrow H_2O + RO^-, \tag{2}$$

where R=CH_3, CH_3CH_2, $(CH_3)_2CH$, and $(CH_3)_3C$ or

$$ROD + OH^- \rightarrow HOD + RO^-, \tag{3}$$

where R=CD_3, CD_3CD_2.

Collisional relaxation via the He buffer gas serves to equilibrate the anions to a vibrational temperature of 300 K. Further cooling to ~200 K is possible by enclosing the afterglow apparatus in a jacket of liquid nitrogen. Anion currents ranged between 10 and 70 pA. Anions are extracted and accelerated through a Wien velocity filter and subsequently decelerated into an interaction region; here the ion beam perpendicularly intersects the laser photons from a fixed frequency ($\lambda = 364$ nm) CW argon ion laser with ~100 W of circulating power in a buildup cavity. Photoelectrons are collected in a small solid angle in a direction perpendicular to the plane of the ion and laser beams. They pass through a hemispherical energy analyzer and onto a position sensitive detector as a spectrum is recorded with a resolution of ~10 meV. The spectra are collected as a function of electron kinetic energy (eKE), which may be converted to electron binding energy (eBE) by subtracting the eKE from the laser photon energy (3.408 eV). The absolute energy scale is fixed by the position of the $^3P_2 \leftarrow {}^2P_{3/2}$ transition in the O^- photoelectron spectrum. An additional small (<1%) energy compression factor is applied as determined from comparison of the photoelectron spectrum of tungsten ion (W^-) with known transitions in tungsten atom.[35]

The CD_3O^- photoelectron spectrum contains contamination from DO_2^- peaks. The flow tube conditions described above also allow for the synthesis of DO_2^- through the reaction of CD_3OD with O_2^-. Because both DO_2^- and CD_3O^- have $m/z = 34$, the DO_2^- could not be eliminated via mass selection. A separate pure DO_2^- photoelectron spectrum was subsequently obtained and was subtracted from the CD_3O^- spectrum.

The polarization of the incident laser beam can be varied by rotating a half-wave plate in the beam path, allowing sampling of the angular distribution of photoelectrons at three laser polarization angles—0° (parallel), 54.7° (magic angle), and 90° (perpendicular) with respect to the electron detection axis. The angular distribution of a spectral peak can be characterized by its asymmetry parameter, β,[36] which

may be calculated by an expression involving the intensity of the peak measured at polarization angles 90° and 0°, $I_{90°}$ and $I_{0°}$, respectively,

$$\beta = \frac{I_{0°} - I_{90°}}{\frac{1}{2} I_{0°} + I_{90°}}, \tag{4}$$

where $-1 \leqslant \beta \leqslant 2$.

To a first approximation, a $\beta \sim 2$ results from a *p*-wave photoelectron, which originates from photodetaching an *s*-like electron. Photodetaching a *p*-like electron produces both *s*-wave and *d*-wave electron distributions. For energies close to the threshold energy of the transition, the *s*-wave contribution will dominate, resulting in a $\beta \sim 0$, although as energy increases, the *d*-wave contribution will become greater and the β will approach -1. In this way, angular distribution information in photoelectron spectra can be used to distinguish between transitions to different electronic states.[37]

Spectra were taken at both 200 K and 300 K (room temperature) vibrational temperature and compared in order to identify transitions originating from vibrationally excited states in the anion. This allows for a confident assignment of the 0_0^0 peak.

Ab initio calculations of both CH_3CH_2O and $(CH_3)_2CHO$ anions and radicals were implemented using the GAUSSIAN94 program package.[38] In CH_3CH_2O, two sets of calculations were employed. The first, referred to as Method 1, used the density functional theory B3LYP method with a 6-31+G* basis set, while the second, Method 2, used the B3LYP method with an aug-cc-pVDZ basis set. In $(CH_3)_2CHO$, Method 2 was employed for the anion and ground state of the radical, but no potential minimum for the first excited state was found. Therefore a third set of calculations was executed using a HF method with an aug-cc-pVDZ basis set for the anion and ground state of the $(CH_3)_2CHO$ radical, and the CIS method with the aug-cc-pVDZ basis set for the first excited state of $(CH_3)_2CHO$. This is referred to as Method 3. The GAUSSIAN94 calculation output files, which include optimized geometries, normal modes, and vibrational frequencies, were then used in the CDECK suite of programs.[39] This package calculates Franck–Condon factors for the possible anion to neutral transitions using a harmonic oscillator approximation, and outputs a stick photoelectron spectrum simulation. This stick spectrum is then convoluted with a 10 meV Gaussian function to produce a simulated spectrum that can be directly compared to the data. If the correspondence between theory and experiment is good, the theoretical output may be used as a guide for understanding and assigning the experimental spectral features. The calculated vibrational frequencies are not scaled unless otherwise stated.

A different procedure, referred to as Method A, was used to simulate the photoelectron spectrum of $(CH_3)_3CO^-$. In this case, the anion and neutral potential energy surfaces were assumed to be harmonic. Experimental frequencies were input, assuming the same frequency in the anion and neutral species for each mode. The change in geometry between the anion and neutral was adjusted in order to reproduce the intensities of the peaks in the experimental spectrum. Finally, the simulated peaks were convoluted with a full-width at half-maximum (FWHM) of 10 meV. No hot bands were simulated.

III. RESULTS AND DISCUSSION

A. CH_3O^-

A detailed theoretical description of Jahn-Teller effects, particularly with respect to CH_3O radical, has recently been given by Barckholtz and Miller.[24] A brief overview is given here. As mentioned above, the ground electronic state of CH_3O has a twofold degeneracy in its C_{3v} geometry configuration. This degeneracy leads to a Jahn-Teller phenomenon; in order to minimize energy, the radical will distort, thus breaking the C_{3v} symmetry and lifting the degeneracy. CH_3O has six vibrational modes. Three are symmetric a_1 modes: ν_1 CH stretch, ν_2 umbrella, and ν_3 CO stretch; and three are asymmetric *e* modes: ν_4 CH stretch, ν_5 HCH scissors, and ν_6 methyl rock, which involves movement of the oxygen off the C_{3v} axis toward one of the hydrogens. The symmetric modes do not provide the distortion necessary to remove the degeneracy and lower the energy, and thus only the asymmetric *e* vibrational modes can be Jahn-Teller active. The methoxy radical is known to exhibit a ''dynamic'' Jahn-Teller effect, where the zero-point energies of the vibrations are much greater than the stabilization energy of the Jahn-Teller distortion.[24] Therefore the distortion is not large enough to provide a permanent departure from C_{3v} to C_s symmetry and must be treated as a vibronic coupling problem where the asymmetric vibrational *e* modes couple to the degenerate *E* electronic states.

The room temperature magic angle, and 0° and 90° photoelectron spectra for CH_3O^- are presented in Figs. 2(a) and 2(b), respectively. Peak a is assigned as the 0_0^0 transition that gives $EA(CH_3O) = 1.572 \pm 0.004$ eV. The magic angle spectrum shows what appears at first glance to be a regular Franck–Condon progression of doublets in peaks a, c and d, g and h, i and j, and k and l. Closer examination of the spacings, however, reveals that this is not the case. The interpeak spacings of c and d, g and h, i and j, and k and l are 255 cm^{-1}, 155 cm^{-1}, 365 cm^{-1}, and 355 cm^{-1}, respectively. Furthermore, the spacing between peaks a and c, c and g, g and i, and i and k are 1210 cm^{-1}, 1530 cm^{-1}, 1195 cm^{-1}, and 1400 cm^{-1}, respectively. In addition, there are the relatively weak peaks b and e whose photoelectron angular distributions differ markedly from the other peaks in the spectrum. Peaks a, c, d, f, and h show similar behavior in the 90° and 0° polarization scans in that their intensities are heavily weighted in the 90° direction [Fig. 2(b)]. This is reflected in the asymmetry parameter values ($\beta \sim -1$) for these peaks listed in Table I. The opposite is true for peaks b and e, whose β values are closer to $+1$. (These values are taken from closeup spectra of the region, which are not shown). Peaks g, i, j, k, and l display essentially isotropic angular distributions and thus $\beta \sim 0$ as given in Table I.

The position and intensity of the magic angle spectrum peaks agree well with a recently published CH_3O^- photoelectron spectrum by Osborn and co-workers.[40] In contrast to

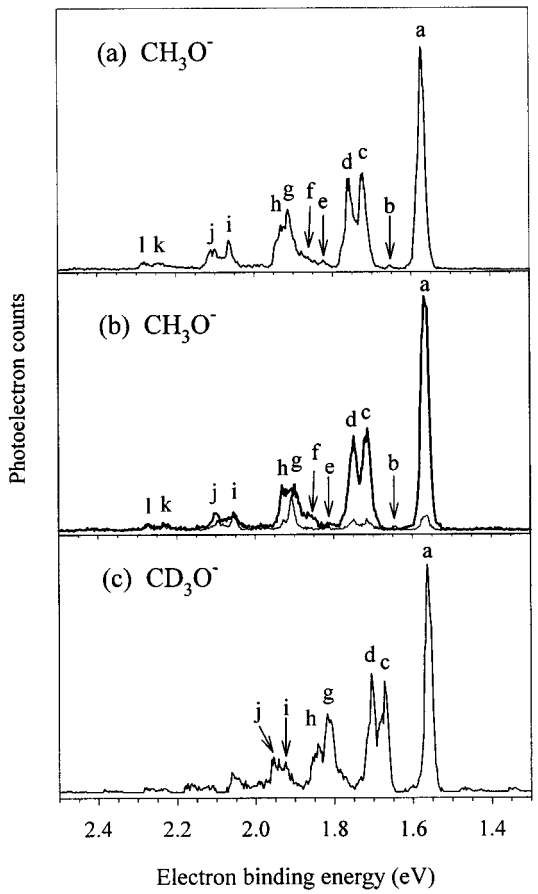

FIG. 2. (a) Magic angle photoelectron spectrum of CH_3O^- taken at 300 K sample temperature. (b) 300 K photoelectron spectrum of CH_3O^- taken at 90° (heavy line) and 0° (light line) polarization angles with respect to the electron detection axis. (c) Magic angle photoelectron spectrum of CD_3O^- taken at 300 K sample temperature, DO_2^- subtracted. See text for details.

the original photoelectron spectra taken of CH_3O^- under significantly poorer resolution,[3] none of the major features in the spectra in Fig. 2(a) are spaced such that they could be assigned to any of the three a_1 symmetric vibrational modes: $\nu_1=2869\ \mathrm{cm}^{-1}$, $\nu_2=1375\ \mathrm{cm}^{-1}$, $\nu_3=1062\ \mathrm{cm}^{-1}$.[14] This leaves only the doubly degenerate *e* vibrational modes ν_4, ν_5, and ν_6; the fact that all the prominent spectral features can be attributed to asymmetric modes testifies to the presence of significant Jahn-Teller effects in CH_3O.

Due to the dynamic nature of the Jahn-Teller effect in CH_3O, *ab initio* calculations using programs such as GAUSSIAN94 that are based on the Born–Oppenheimer approximation are not feasible as they do not account for the vibronic coupling of electronic and vibrational energy levels. For this reason, and to understand more about the photoelectron spectrum of CH_3O^-, we compare our peak positions with those observed by Temps[19] who has cataloged and assigned vibronic symmetry to lines observed in rotationally resolved SEP/LIF studies of CH_3O and CD_3O.

We are able to use the information provided by the β parameters as discussed above, in addition to Temps' results, to make assignments (see Table I). The 0_0^0 transition, peak a, necessarily carries an *E* vibronic symmetry assignment. This is because the degenerate *E* symmetry of the electronic state

TABLE I. Peak positions, asymmetry (β) values, and assignments for the photoelectron spectrum of CH_3O^-. Errors on β values are ± 0.1. Assignments are made to SEP peak positions (cm^{-1}) and vibronic symmetries given in Ref. 19. See text for details.

Peak	Position (cm^{-1})	β	Assignment
a	0	−0.9	$0\ 0_0^0(E)$
b	630±10	⩾1.2	$652\ 6_0^1(A_1)$
c	1210±10	−0.9	$1198\ 6_0^1(E)$
d	1465±10	−0.8	$1490\ 5_0^1(E)$
e	2015±30	⩾1.0	$2018\ 2_0^1 6_0^1(A_1)$
f	2450±90	−0.8	$2432\ 2_0^1 3_0^1(E)$
			$2441\ 5_0^1 6_0^1(E)$
			$2488\ 6_0^3(E)$
g	2740±10	−0.2	$2730\ 5_0^2(E)$
			2750 ?
			$2760\ 2_0^1 5_0^1(A_1)$
h	2895±10	−0.7	$2862\ [5_0^2/4_0^1(E)]$
i	3935±10	−0.1	⋯
j	4300±10	−0.3	⋯
k	5335±30	−0.1	⋯
l	5690±15	−0.1	⋯

couples with the totally symmetric vibrationless level to give *E* vibronic symmetry, $E\otimes a_1=E_{\mathrm{vibronic}}$. Peaks b, c, and d are assigned to the 6_0^1 (A_1), the 6_0^1 (E), and the 5_0^1 (E) vibronic lines, respectively. Peaks a, c, and d ($\beta\sim-1$) are all assigned to *E* vibronic symmetry while peak b ($\beta\geqslant 1.2$) has *A* symmetry; this suggests a strong correlation between asymmetry parameters and the vibronic symmetry assignment given to the final state involved in the anion to neutral transition. Furthermore, the *A* vibronic peak has an intensity significantly smaller than that of its neighboring peaks of *E* symmetry. With this in mind, peak e is assigned to the $2_0^1 6_0^1$ (A_1) transition at 2018 cm^{-1}, as its β value and relative intensity is similar to that of peak b.

A similar phenomenon was observed[41] in the photoelectron spectrum of C_2H^-. In this case, the spectrum was dominated by peaks assigned to Franck–Condon-allowed transitions. However, structure on a scale approximately 50 times smaller than the origin transition was observed, which was attributed to non-Franck–Condon transitions into odd quanta of asymmetric modes in the ground state of the radical. In addition, the non-Franck–Condon peaks displayed asymmetry parameters with opposite sign as the peaks corresponding to activity of symmetric modes of the neutral. These normally forbidden transitions gain intensity via an electronic state mixing between the ground state of the neutral and an excited electronic state. The same mechanism is proposed to explain anomalous intensities in the $\tilde{A}\,^2A_1\leftrightarrow\tilde{X}\,^2E$ excitation spectrum of methoxy radical.[17,42] In the LIF studies, for peaks involving modes of *e* vibrational symmetry, normally forbidden parallel transitions are observed with intensities of comparable magnitude to the allowed perpendicular transitions. Here the electronic state mixing is suggested to be between the $\tilde{A}$ state and a closely lying excited *E* electronic state. In the case of the CH_3O^- photoelectron spectrum, the ground *E* electronic state of the radical may mix with an excited electronic state although the first excited state lies several eV above the ground state.

Peak f, which falls at 2450 cm^{-1}, has the same β value as peaks a, c, and d. It may correspond to either the $2_0^1 3_0^1$ (E) line at 2432 cm^{-1}, the $5_0^1 6_0^1$ (E) line at 2441 cm^{-1}, or the 6_0^3 (E) line at 2488 cm^{-1}. Due to its breadth, peak f may obtain intensity from any or all of these lines. At 2740 cm^{-1} above the origin lies peak g. Its β value is closer to zero than the previous large-intensity peaks mentioned with significant intensity. This suggests that peak g is a mix of peaks with E and peaks with A_1 vibronic symmetry. The possibilities are the 5_0^2 (E) line at 2730 cm^{-1}, a line of undetermined symmetry at 2750 cm^{-1}, and the $2_0^1 5_0^1$ (A_1) line at 2760 cm^{-1}. Peak h falls into the same category as peaks a, c, d, and f at 2895 cm^{-1}. Its assignment is either the 2862 cm^{-1} line {this line was given a tentative vibronic label of $[5_0^2/4_0^1$ $(E)]$ (Ref. 19) which is distinguished by its brackets in Table I}, or the 4_0^1 (E) transition at 2889 cm^{-1}. Lines with excitation energies greater than 3000 cm^{-1} are not assigned. The higher the transition lies in the $\tilde{X}\,^2E$ potential well, the more vibronic mixing there is, rendering it too difficult to determine vibronic symmetry past this energy.[19]

It should be emphasized that the photoelectron spectrum of CH_3O^- is dominated by the Jahn-Teller-active (asymmetric) vibrational modes and the normally expected features due to vibrations solely of symmetric modes are absent. Peaks e, f, and g carry assignments involving combination bands of symmetric and asymmetric vibrational modes. Thus we do see activity of the symmetric modes in the CH_3O^- photoelectron spectrum, although only when coupled with motion from the asymmetric modes.

The spin–orbit splitting of the ground state of methoxy radical is 61.5 $\pm$1.0 cm^{-1} ($\sim$7 meV),[1,43] which is less than the resolution of our experiment. Nevertheless, the spin–orbit splitting contributes to the widths of the peaks observed. The FWHM of peaks a, c, and d in the cold magic angle spectrum of CH_3O^- are 172, 158, and 102 cm^{-1}, respectively. As energy increases, the spin–orbit splitting is quenched, as expected.[22,24] Both spin–orbit and Jahn-Teller interactions compete for orbital angular momentum and as the Jahn-Teller energy interaction increases at higher energies in the potential well, the spin–orbit splitting should necessarily decrease.

B. CD_3O^-

The room temperature deuterated methoxide spectrum with DO_2^- subtracted (see Experiment) is shown in Fig. 2(c). Peak a, the 0_0^0 transition, falls at an energy of 1.559$\pm$0.004 eV.

At first glance, we see the same coarse structure in CD_3O^- as in CH_3O^- in that the intensity pattern and the relative spacings are the same. The peaks appear to have uniformly shifted to smaller binding energy; in fact, if a one-to-one correspondence is assumed between peaks a, c, d, g, h, i, and j in both spectra, which is not intuitively unreasonable, all of these peaks shift their position in an essentially uniform manner relative to peak a by between 21% and 26%. This agrees with the findings in the recent photoelectron spectrum of CD_3O^-.[40] A vibrational mode that involves a large amount of hydrogen movement would decrease in frequency upon substituting hydrogen with deuterium and thus a photoelectron peak would shift to lower binding energy. A mode that involves little or no hydrogen movement will not shift. The CO stretch, ν_3, is the only mode of CD_3O that falls into this category. Therefore the evidence indicates that we are not seeing any activity in the symmetric ν_3 mode.

TABLE II. Peak positions, asymmetry (β) values, and assignments for the photoelectron spectrum of CD_3O^-. Errors on β values are $\pm$0.1. Assignments are made to SEP peak positions (cm^{-1}) and vibronic symmetries given in Ref. 19.

Peak	Position (cm^{-1})	β	Assignment
a	0	−0.9	0 0_0^0 (E)
c	920$\pm$15	−0.9	885 $6_0^1(E)$
d	1160$\pm$15	−0.9	1172 $5_0^1(E)$
g	2035$\pm$15	−0.6	1995 $5_0^2(E)$
h	2275$\pm$20	−0.8	? $[5_0^2 4_0^1$ $(E)]$
i	2920$\pm$15	−0.4	⋯
j	3180$\pm$20	⋯	⋯

We should be able to use the information provided by the β parameter signature of the peaks to further corroborate the apparent one-to-one correspondence and make assignments. Assignments for CD_3O are made in the same manner as discussed in CH_3O, i.e., matching our lines to those of Temps LIF/SEP studies of CD_3O (Ref. 19) taking into account both the position and the β parameter/symmetry of the peak as reported in Table II. In the case of peaks a, c, d, and h, the β parameter values for the peaks in both the CH_3O^- and CD_3O^- spectra are essentially identical; this provides additional confirmation that peaks a, c, d, and h in the CH_3O^- and CD_3O^- spectra can be attributed to the same set of transitions. Peaks c and d are assigned to 6_0^1 (E) and 5_0^1 (E), respectively, as is seen in peaks c and d in CH_3O^-. Peak g, however, has a β of -0.2 in CH_3O^- but a β of -0.6 in CD_3O^-, which is a significant change in asymmetry parameter. It is likely that the three vibronic lines that were assigned to peak g in the CH_3O^- spectrum shifted, but by different amounts. The shifts could happen in such a way that the 5_0^2 (E) line no longer overlaps with an A line, and therefore its β looks more like peaks c and d. Peak g is therefore assigned to the 5_0^2 (E) line of CD_3O^- at 1995 cm^{-1}. This further supports the assignments for peak g in CH_3O^-.

Peaks h in both spectra have similar asymmetry values, and therefore are confirmed to be the same peak, either the $[5_0^2/4_0^1$ $(E)]$ line or the 4_0^1 (E) line assigned in CH_3O^-. However, the 4_0^1 (E) assigned position does not match peak h in CD_3O^-, so both peaks h obtain the $[5_0^2/4_0^1$ $(E)]$ assignment. The Temps assignments for CD_3O terminate around 2200 cm^{-1},[19] so we are not able to confirm the assignment of the CD_3O peak h as the $[5_0^2/4_0^1$ $(E)]$ line. Peak i in CD_3O has changed its value of β significantly, so it is possible that the peak i in CH_3O is composed of several different lines which shift by different amounts upon deuteration, as has been discussed above for peak g.

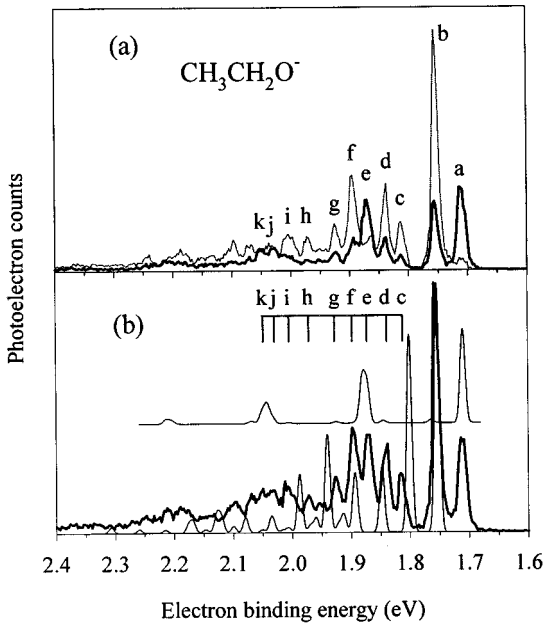

FIG. 3. (a) 200 K $CH_3CH_2O^-$ photoelectron spectrum taken at 90° (heavy line) and 0° (light line) polarization angles with respect to the electron detection axis. (b) The 200 K $CH_3CH_2O^-$ magic angle photoelectron spectrum is displayed in bold. The thin line at the baseline corresponds to Method 2 (B3LYP/aug-cc-pVDZ) simulation of the photoelectron transition into the $\tilde{A}$ state of CH_3CH_2O as described in the text. The floated line is the simulation of the photoelectron transition into the $\tilde{X}$ state of CH_3CH_2O.

C. $CH_3CH_2O^-$ and $CD_3CD_2O^-$

The 90° and 0° polarization photoelectron spectra of 200 K $CH_3CH_2O^-$ are shown in Fig. 3(a). No structure in the $CH_3CH_2O^-$ photoelectron spectra could be attributed to hot bands. Peak a is assigned as the EA at 1.712 ± 0.004 eV.

Examination of the spectra shows that there are two groups of peaks with contrasting β parameters (see Table III). The first group, which includes peaks a and e, possesses a $\beta < 1$, while peaks b–d and f–i have opposite angular distributions, $\beta > 1$. The existence of the two groups of β values indicates that they correspond to different electronic states. This is strong evidence supporting the presence of a low-lying first excited state of ethoxy radical. Peaks a and e correspond to transitions from the ground state of $CH_3CH_2O^-$ anion into the ground state of neutral CH_3CH_2O, while peaks b–d, and f–i represent transitions into the first excited state of the neutral. Therefore, the spacing between peaks a and b, 355 ± 10 cm^{-1}, determines the term energy of the first excited state. To our knowledge, this quantity has never before been directly measured, although there has been a laser fluorescence study of CH_3CH_2O that did not observe any excited states within 300 cm^{-1} of the ground state.[27] The direct observation of the ground to first excited state spacing in the radical supports the substitution argument previously mentioned. The substitution of one hydrogen of CH_3O with a methyl group perturbs the C_{3v} geometry and thus slightly lifts the electronic degeneracy present in methoxy radical.

TABLE III. Peak positions, asymmetry (β) values, and assignments for the photoelectron spectrum of $CH_3CH_2O^-$ and $CD_3CD_2O^-$. Errors on β values are ± 0.1.

$CH_3CH_2O^-$			$CD_3CD_2O^-$		
Peak	Position (cm^{-1})	β	Peak	Position (cm^{-1})	β
a	0	−0.8	a	0	−0.7
b	355±10	0.9	b	275±10	0.9
c	830±10	0.9	c	660±20	1.2
d	1040±10	0.7	d	805±10	0.6
e	1295±10	−0.4	e	1090±10	0.2
f	1490±10	0.8	f	1380±15	0.8
g	1730±10	0.7	g	1915±15	0.5
h	2110±15	0.9	h	2135±10	0.1
i	2365±15	0.6	i	2360±15	0.6
j	2575±10	0.1			
k	2740±15	−0.1			

The spacing between peaks a and e is 1295 cm^{-1} and two quanta falls at 2590 cm^{-1}, which is in the vicinity of peaks j and k. The fact that the β values for peaks j and k are the same within error, however, indicates that the second quantum transition is contributing to both these peaks, and therefore they receive the same assignment in the ground state of the radical. The spacings between peaks b and d matches that of peaks d and g, ~ 685 cm^{-1}. Furthermore, the intensity pattern between peaks b, d, and g matches that of a typical Franck–Condon progression and therefore these peaks are assigned as a vibrational progression in the first excited state of the radical. The relationship between the remaining peaks, aside from which electronic state in the radical they belong to, is unclear.

Comparison of the observed spectrum with information provided by *ab initio* calculations of CH_3CH_2O and $CH_3CH_2O^-$ can help clarify and confirm the above observations. Method 2 (B3LYP/aug-cc-pVDZ) calculates the anion to be a $^1A'$ state, while the radical has a $^2A''$ ground state with a $^2A'$ first excited electronic state predicted to lie 360 cm^{-1} higher. This spacing is in good agreement with the observed difference between peaks a and b.

The CDECK simulation of the photoelectron spectrum of $CH_3CH_2O^-$ using the results from Method 2 is presented in Fig. 3(b) along with the magic angle photoelectron spectrum taken at 200 K sample temperature. The simulation at the baseline represents the first excited state results while the floated plot represents the ground state simulation. The positions and intensities of the 0_0^0 peaks in the simulations (peaks a and b) are fixed to match the experimental peaks (in bold).

Method 2 predicts the most active mode in the $\tilde{X}\,^2A'' \leftarrow \tilde{X}\,^1A'$ photoelectron spectrum to be ν_9 at 1303 cm^{-1}, a symmetric scissor motion of the nonmethyl hydrogens. As is shown in Fig. 3(b), the simulation has excellent agreement for the intensity of peak e with respect to peak a, as well as the intensities of peaks j/k with respect to peak a. These peaks are therefore given the assignment of 9_0^1 and 9_0^2, respectively.

The agreement between the excited state calculation and experiment is not as conclusive, however. For example, the predicted intensity of peak c is highly overestimated. Furthermore, peaks c and d are predicted to form a progression in a single mode, and from examining their intensities in the experimental spectrum, this is not obviously true. This would

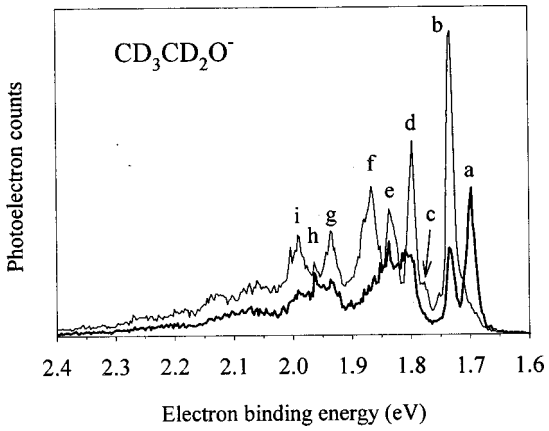

FIG. 4. 300 K $CD_3CD_2O^-$ photoelectron spectrum taken at 90° (heavy line) and 0° (light line) polarization angles with respect to the electron detection axis.

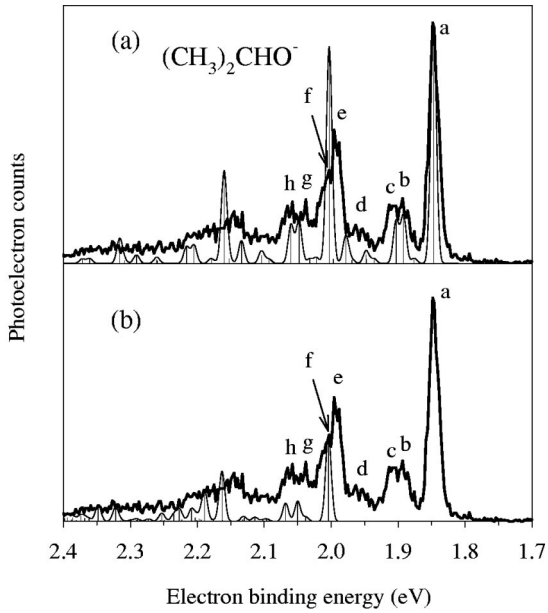

FIG. 5. (a) The 200 K magic angle photoelectron spectrum of $(CH_3)_2CHO^-$ is displayed in bold. The thin line corresponds to a theoretical simulation using Method 1 (B3LYP/6-31+G*) of the photoelectron transition into the $\tilde{X}$ state of $(CH_3)_2CHO$. (b) The 200 K magic angle photoelectron spectrum of $(CH_3)_2CHO^-$ is displayed in bold. The thin line corresponds to a theoretical simulation using Method 3 (CIS/aug-cc-pVDZ) of the photoelectron transition into the $\tilde{A}$ state of $(CH_3)_2CHO$.

also conflict with the implication that peaks d and g form a vibrational progression. Peak f lines up well with the simulation peak corresponding to the fundamental of ν_7, the CO stretch predicted at 1118 cm^{-1}. However, it is unclear which simulated peak to match to peak g. For features to higher binding energy of peak g (and including peak g), the agreement with the simulation is ambiguous. In short, the less-than-ideal match between the experimental intensities and spacings and those derived by theoretical means does not help us to assign the remaining peaks. This lack of agreement is not completely unexpected, however. If the ground and first excited states of CH_3CH_2O are separated by only 355 cm^{-1}, the two states should couple together strongly with the effect of perturbing vibrational levels away from a harmonic oscillator approximation, and the intensities of the transitions may be affected as well. Therefore, peaks d and g are tentatively assigned as the first and second quanta in a vibrational progression in the $\tilde{A}$ state whose motion is undetermined, while peak f may correspond to the fundamental of ν_7.

The 0° and 90° polarization spectra of $CD_3CD_2O^-$ are shown in Fig. 4. Peaks a and b have similar relative angular distributions and intensities as peaks a and b in $CH_3CH_2O^-$, and the spacing has decreased to 275 ± 10 cm^{-1} (see Table III). As in $CH_3CH_2O^-$, peaks a and b are assigned to the 0_0^0 transitions into the ground and first excited state of the radical, respectively. Peak a is assigned as the EA at 1.699 ± 0.004 eV.

In contrast to the $CH_3CH_2O^-$ photoelectron spectrum, there is no peak that may be grouped with peak a as having similar β parameter. The mode assigned in the ground state of the ethoxy radical, ν_9 at 1303 cm^{-1}, is predicted by Method 2 to shift to 965 cm^{-1} upon deuteration. There is no match for such a peak in the $CD_3CD_2O^-$ experimental spectrum. Method 2 also calculates that the mode ν_7 tentatively assigned to the $CH_3CH_2O^-$ photoelectron spectrum at 1118 cm^{-1} would shift to 987 cm^{-1}. This may correspond to peak e in the $CD_3CD_2O^-$ spectrum.

Comparison of the $CH_3CH_2O^-$ and $CD_3CD_2O^-$ photoelectron spectra suggests that many of the features of the $CH_3CH_2O^-$ spectrum have been crowded together due to the shifting expected upon deuteration. There are fewer features in the $CD_3CD_2O^-$ spectrum, and for peaks to the higher binding energy of peak d, the line shapes are such that they appear to be formed from several peaks. This blending would also affect the intensities of the observed features and their asymmetry parameters. Unlike in the CH_3O^- photoelectron spectrum, we are not able to make a visual correspondence between peaks in the deuterated and nondeuterated spectra. As was the case in $CH_3CH_2O^-$, aside from the few assigned transitions, the simulated spectrum did not accurately reproduce either the relative spacings or the intensities of the spectral features in a consistent manner. Therefore, the congestion observed in the photoelectron spectrum of $CD_3CD_2O^-$ hinders any possible corroboration with structure in the spectrum of $CH_3CH_2O^-$.

In the $CH_3CH_2O^-$ photoelectron spectrum no signature of dissociation of the species is observed. Photodissociation of $CH_3CH_2O^-$ has been observed with a 2.331 eV photon with a low branching ratio of dissociative to stable products.[44]

D. $(CH_3)_2CHO^-$

The magic angle spectrum for $(CH_3)_2CHO^-$ at 200 K sample temperature is displayed in Fig. 5. The β parameters for all the peaks in the $(CH_3)_2CHO^-$ spectrum are essentially identical, spreading over a small range between 0.1 and 0.5. For this reason the polarization spectra are not shown.

The observed peaks and their positions in the $(CH_3)_2CHO^-$ photoelectron spectrum are given in Table IV. The electron affinity for $(CH_3)_2CHO$, corresponding to the

TABLE IV. Peak positions and assignments for the photoelectron spectrum of $(CH_3)_2CHO^-$.

Peak	Position (cm^{-1})	Assignment
hot band	-330 ± 25	$3'^0_1$
a	0	$0^0_0\,\tilde{X}\,^2A'\leftarrow\tilde{X}\,^1A'$
b	375 ± 25	3^1_0
c	500 ± 15	5^1_0
d	925 ± 50	See text
e	1175 ± 15	$0^0_0\,\tilde{A}\,^2A''\leftarrow\tilde{X}\,^1A'$ or 14^1_0
f	1270 ± 20	$0^0_0\,\tilde{A}\,^2A''\leftarrow\tilde{X}\,^1A'$ or 14^1_0
g	1545 ± 15	$\tilde{X}\leftarrow\tilde{X}\,3^1_0 14^1_0+\tilde{A}\leftarrow\tilde{X}\,4^1_0$
h	1740 ± 40	$\tilde{X}\leftarrow\tilde{X}\,5^1_0 14^1_0+\tilde{A}\leftarrow\tilde{X}\,5^1_0$

position of peak a, is 1.847 ± 0.004 eV. The Method 1 calculation predicts an anion with a $^1A'$ ground state and C_s symmetry. The neutral ground state is calculated as a $^2A'$ state with C_s geometry. A peak measured from the room temperature photoelectron spectrum (not shown) is assigned as the hot band transition $3'^0_1$, where ν'_3 is the CCC bend predicted at 360 cm^{-1} in the anion. The CDECK simulation of the photoelectron transition into the ground state radical using results from Method 1 is displayed in Fig. 5(a). The spectrum simulation reproduces both the spacing and intensity of many of the spectral features relatively well. Peak b corresponds to one quantum of vibration in ν_3, predicted at 360 cm^{-1}, which is the CCC bending motion in the radical. Peak c is assigned to one quantum of ν_5, a CCCO symmetric bending mode, which Method 1 calculates at 452 cm^{-1}. Peak d is the result of several transitions. The one with the greatest intensity is the fundamental of ν_{10}, a rocking motion of all hydrogens, predicted to fall at 1054 cm^{-1}. In addition there is a smaller peak to lower binding energy which is primarily composed of overtones and combination bands of ν_3 and ν_5.

The simulation predicts the most active vibration to be ν_{14}, the CO stretch, to lie at 1262 cm^{-1} above the 0^0_0 transition. This is a better match with the position of peak f (1270 cm^{-1}) than peak e (1175 cm^{-1}). However, because peak e is the most intense peak in the spectrum after peak a, the simulated peak may also be assigned to peak e. Therefore it is not clear if it is peak e or peak f that corresponds to 14^1_0. The observation of the CO stretch is expected because detaching an electron localized on the oxygen should affect the CO bond and thus activate the CO stretch. However, unlike the $CH_3CH_2O^-$ spectrum, we are not able to use peaks with contrasting β values to distinguish between different electronic states. What is clear, however, is that the peak that is not assigned to 14^1_0 is absent from the photoelectron spectrum simulation of the transition into the ground state of $(CH_3)_2CHO$. Thus either peak e or f is the 0^0_0 transition from the ground state anion into the first excited state of the neutral. The term energy of the $\tilde{A}$ state is therefore assigned as the average of the positions of peak e and f, 1225 ± 65 cm^{-1}. This spacing is believable in light of the substitution argument applied above. Specifically, replacing two of the hydrogens in CH_3O with methyl groups can be considered a perturbation that lifts the degeneracy of the CH_3O $\tilde{X}\,^2E$ state to a greater degree than in CH_3CH_2O.

The assignment of transitions into the first excited state of $(CH_3)_2CHO$ can be further supported by *ab initio* calculations. Method 3 (HF/CIS/aug-cc-pVDZ) predicts that the anion has a $^1A'$ ground state with C_s geometry and that the neutral has a $^2A'$ ground state with C_s geometry, in agreement with Method 1. The CIS calculation additionally predicts that the first excited state is a $^2A''$ state with C_s geometry, 2011 cm^{-1} above the $\tilde{X}\,^2A'$ state. This agrees fairly well with our measurement of the term energy of the excited state. The CDECK simulation of the photoelectron spectrum using the results from the Method 3 calculation is displayed in Fig. 5(b). In this figure, the intensity and position of the 0^0_0 simulation peak are fixed to match peak f, although choosing between peaks e and f is arbitrary, as discussed above. It is clear that both peaks g and h are composed of transitions into both the $\tilde{X}$ and $\tilde{A}$ electronic states of the radical. Peak g is assigned to the overtone combination $3^1_0 14^1_0$ in the ground state radical plus 4^1_0 in the first excited state, the CCC bend, predicted to fall 371 cm^{-1} above the $0^0_0\,\tilde{A}\leftarrow\tilde{X}$ transition. Similarly, peak h results from the overtone of $5^1_0 14^1_0$ ground state modes plus 5^1_0 in the $\tilde{A}$ state, the CCCO symmetric bend, predicted at 516 cm^{-1}. Beyond peak h the convolution of features from transitions into both ground state and first excited states in the radical is too complex to make unambiguous assignments.

It is interesting that our calculations predict a $^2A''$ ground state with a $^2A'$ first excited state in ethoxy radical, while in isopropoxy radical, the two states are reversed. This is in agreement with the rotational spectroscopy of Foster *et al.*[10] They postulate that this is because in CH_3CH_2O, the nonbonding a' orbital that lies in the C_s plane is closer to the methyl group; in $(CH_3)_2CHO$, the a' orbital is closest to the nonmethyl hydrogen and it is the out-of-plane a'' orbital that has the maximum opportunity for interaction with the two methyl groups. The ordering of the states observed here implies that the proximity of a lone-pair orbital to a methyl group serves to lower its energy relative to the other lone-pair orbital.

E. $(CH_3)_3CO^-$

The magic angle photoelectron spectrum of $(CH_3)_3CO^-$ at 200 K is displayed in Fig. 6. As was the case for $(CH_3)_2CHO^-$, there is essentially no variation in β parameter over the span of the spectrum, as it ranges between 0.1 and -0.3.

Peak b is measured at 435 cm^{-1} above the 0^0_0 transition. This is the same spacing between peaks b and c, peaks d and e, and peaks e and f. This suggests that peaks b and c form a vibrational progression in one mode, and peaks e and f form the same vibrational progression in combination with peak d. Peak d falls at 1205 cm^{-1} above peak a, and peak g lies at twice that amount, implying that peaks d and g form a second vibrational progression.

Because $(CH_3)_3CO$ is expected to exhibit Jahn-Teller effects due to its C_{3v} geometry and concomitant degenerate $\tilde{X}\,^2E$ electronic ground state,[6] we were unable to carry out

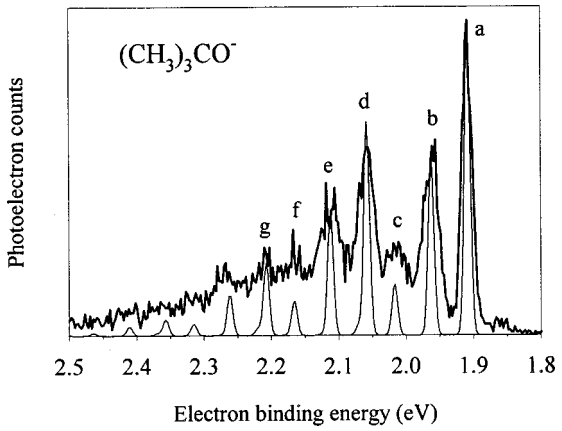

FIG. 6. Magic angle photoelectron spectrum of $(CH_3)_3CO^-$ taken at 200 K sample temperature in bold. The thin line corresponds to a Franck–Condon simulation of the photoelectron spectrum in a simple harmonic oscillator approximation using experimental frequencies (Method A). See text for details.

our own calculations on $(CH_3)_3CO$ using *ab initio* methods based on the Born–Oppenheimer approximation. However, recently Barckholtz and Miller have outlined a method for *ab initio* calculations that includes coupling between electronic and vibrational wave functions and is therefore able to compute spectroscopically observable parameters of Jahn-Teller species.[45] A calculation for $(CH_3)_3CO$ using this above method[46] corroborates the assignments proposed above (see Table V). It predicts the symmetric a_1 CCC umbrella mode ν_6 at 389 cm^{-1} and the a_1 mode ν_{18} at 1234 cm^{-1} which is the CO stretching motion. In the anion, mode ν_6' corresponds to the same CCC umbrella motion as the radical mode ν_6, and is predicted at the slightly lower frequency of 381 cm^{-1}. A peak was measured from the room temperature photoelectron spectrum (not shown) at 440 cm^{-1}, which we assign as a hot band resulting from excitation from $6'^0_1$. The observation of the CO stretch is expected for the same reason discussed in $(CH_3)_2CHO$.

Figure 6 displays a spectral simulation created using Method A. The experimental frequencies of 435 and 1205 cm^{-1} are input to produce the displayed curve. The agreement is surprisingly accurate considering the relative crudeness of the simulation for such a theoretically complicated species. This point will be discussed further below.

TABLE V. Peak positions and assignments for the photoelectron spectrum of $(CH_3)_3CO^-$.

Peak	Position (cm^{-1})	Assignment
hot band	-440 ± 25	$6'^0_1$
a	0	0^0_0
b	435 ± 15	6^1_0
c	855 ± 25	6^2_0
d	1205 ± 15	18^1_0
e	1625 ± 45	$18^1_0 6^1_0$
f	2080 ± 30	$18^1_0 6^2_0$
g	2410 ± 30	18^2_0

F. Vibronic coupling and Jahn-Teller effects

As was stated above in the discussion of ethoxy radical, the majority of the vibrational features in the $CH_3CH_2O^-$ photoelectron spectrum exhibit irregular frequency and intensity patterns that the reasonably high-level calculations and simulations fail to accurately reproduce. This has been attributed to the vibronic coupling between the ground and first excited states in the radical, separated by only 355 cm^{-1}. In the photoelectron spectrum of $(CH_3)_2CHO^-$, however, regularly spaced series of peaks are observed that, with the help of theoretical simulations, can be explained and assigned. In $(CH_3)_2CHO$, the excitation to the first excited state (1225 cm^{-1}) is approximately three times greater than in CH_3CH_2O; therefore the degree of coupling between the $\tilde{X}$ and $\tilde{A}$ states of $(CH_3)_2CHO$ would be expected to be smaller. In addition, however, one must consider the magnitude of the frequencies involved with respect to the energy splitting between the interacting electronic states. In $(CH_3)_2CHO$, the majority of the assigned peaks—b, c, d, and possibly e—fall at energies less than the energy where the $\tilde{A}$ state begins. Therefore, vibronic coupling effects would be expected only for peaks at greater binding energies than peaks e or f. In ethoxy radical this is not the case. The splitting between the electronic states of the neutral is small enough that all of the observed features are subject to vibronic coupling effects.

The existence of the signature of vibronic coupling upon the frequency and spacings of the photoelectron features can be explained, and this may be the reason for the variation of β in the $CH_3CH_2O^-$ spectrum and not in $(CH_3)_2CHO^-$. The relative ordering of the a' and a'' orbital energy is switched between CH_3CH_2O and $(CH_3)_2CHO$, but both orbitals show the same $p\pi$ character. Therefore there is no reason to first order why transitions to the ground and first excited states, corresponding to detaching electrons from the a' and a'' orbitals, would exhibit different angular distributions, which is the case for $(CH_3)_2CHO$, but not for CH_3CH_2O. Thus the different angular distribution behavior for the two species must be originating from another source. In the CH_3O^- photoelectron spectrum, electronic state coupling is proposed to explain intensity in peaks which have different angular distributions than the other peaks in the spectrum. It is possible that the same kind of mixing can explain the angular distribution variation for peaks in the $CH_3CH_2O^-$ spectrum through coupling either between the $\tilde{X}$ and $\tilde{A}$ states of the radical, or between either of these states and a third electronic state.

The relationship of $(CH_3)_3CO$ to CH_3O with respect to the prominence of Jahn-Teller effects in the photoelectron spectra is similar to that between CH_3CH_2O and $(CH_3)_2CHO$ with respect to vibronic coupling effects. The CH_3O^- photoelectron spectrum is dominated by activity in the *e* asymmetric modes falling at positions determined by the Jahn-Teller coupling parameters of the radical. In $(CH_3)_3CO$, however, the major structure is assigned to harmonic progressions in symmetric a_1 vibrational modes. Furthermore, the method used for simulation of the spectrum in Fig. 6 only allows for optimization of a limited number of

TABLE VI. Electron affinities (EA) in eV. Values have been rotationally corrected. See text for details.

Species	EA (eV)	Literature value	Reference
CH_3O	1.572 ± 0.004	1.568 ± 0.005	40
CD_3O	1.559 ± 0.004	1.551 ± 0.005	40
CH_3CH_2O	1.712 ± 0.004	1.715 ± 0.007	26
CD_3CD_2O	1.699 ± 0.004	1.703 ± 0.007	26
$(CH_3)_2CHO$	1.847 ± 0.004	1.839 ± 0.029	25
$(CH_3)_3CO$	1.909 ± 0.004	$1.912^{+0.029}_{-0.054}$	25

free parameters strictly within the Born–Oppenheimer approximation and nevertheless provides a surprisingly accurate simulation of the photoelectron spectrum. This does not mean, however, that there is no Jahn-Teller activity in the $(CH_3)_3CO$ radical. A simulation of the Jahn-Teller active modes in the $(CH_3)_3CO$ spectrum indicates that the most prominent Jahn-Teller transitions have an intensity of about 10% of the origin transition.[46] Although $(CH_3)_3CO$ is expected to be Jahn-Teller-active, the activity is predicted to be small, which is what we observe in our spectrum. The greater amount of vibrational activity in the larger $(CH_3)_3CO$ radical, as well as the resolution of our experiment, produces a baseline of intensity under which any Jahn-Teller transitions may lie. This may include transitions into pure *e* vibrational modes as well as any combinations of symmetric and asymmetric modes. The fact that the gross structure of the $(CH_3)_3CO^-$ photoelectron spectrum may be assigned to regularly spaced transitions into symmetric vibrational modes characterizes this species more closely with $(CH_3)_2CHO$ than CH_3O. Furthermore, the asymmetry parameter behavior of $(CH_3)_2CHO$ and $(CH_3)_3CO$ is similar because β is constant across the spectrum. In light of these parallels, it may prove more fruitful to think of $(CH_3)_2CHO$ as a geometrical perturbation away from the $(CH_3)_3CO$ structure, where one methyl group as been substituted by a hydrogen.

G. Thermochemistry

The EAs for each neutral in this study are reported in Table VI. The EAs have been rotationally corrected and the error bars account for energy compression, rotational broadening, and measurement fitting error. The table lists previous photoelectron spectrum determinations of the EA for comparison. In each case, agreement with the prior studies is good and the error bars have improved. In the case of $(CH_3)_2CHO$ and $(CH_3)_3CO$, the error bars have improved dramatically, by a factor of at least 7.

The RO EAs from this work may be used together with literature values of the gas-phase acidity (GPA) of ROH (Refs. 26,47–50) and the ionization potential of the hydrogen atom in a thermochemical cycle to determine the bond dissociation energy, D_{300}(RO–H),[51] where R=CH_3, CD_3, CH_3CH_2, CD_3CD_2, $(CH_3)_2CH$, and $(CH_3)_3C$. Because the ionization potential of the hydrogen atom and the RO EAs were measured at 0 K, and the GPAs of ROH were measured at 300 K, a thermal correction to the bond dissociation energy was incorporated into the values calculated in Table VII.[51] The GPAs chosen were the directly determined experimental values with the best error bars, where available, and those used for R=CH_3, $(CH_3)_2CH$, and $(CH_3)_3C$ are not significantly different than those measured in deTuri *et al.*[49] The calculated bond dissociation energy values (see Table VII) agree well with those of deTuri *et al.*,[49] who have used the EAs reported in this work with their GPAs to calculate bond dissociation energies. We find that within the given error bars, the energy needed for the reaction ROH→RO+H is relatively independent of R, where R is an aliphatic hydrocarbon.

In addition, literature values for $\Delta_f H_{300}$(H) and $\Delta_f H_{300}(H^+)$,[52] $\Delta_f H_{300}$(ROH),[53] and IP_0(RO) (Refs. 54–56) allow calculation of the heats of formation for the undeuterated RO, RO^-, and RO^+ species according to the methods outlined in Ref. 51. The $\Delta_f H_{300}$(RO) and $\Delta_f H_{300}(RO^-)$ values show a stabilization effect with an increase in the size of R. This effect is greater in the anion than in the radical, a result of inductive effects in the anion. The differences in the amount of stabilization in the anion with respect to the neutral may be examined most precisely by looking at the differences in the EAs. The EA changes by the same amount when going from CH_3O to CH_3CH_2O as when going from CH_3CH_2O to $(CH_3)_2CHO$, but the difference between the

TABLE VII. Derived thermochemical data. Values were computed with literature values for $\Delta_{acid}H_{300}$(ROH) and electron affinities from this work as outlined in Ref. 51. Numbers in parentheses are offered as alternative values originating from independent determinations. All values are in kJ/mol.

R	$\Delta_{acid}H_{300}$(ROH)	D_{300}(RO–H)	$\Delta_f H_{300}$(RO)	$\Delta_f H_{300}(RO^-)$	$\Delta_f H_{300}(RO^+)$
CH_3	1600 ± 2[a]	440 ± 3	21 ± 4	-138 ± 2	1060 ± 10
CD_3	1597 ± 8[b]	436 ± 9	⋯	⋯	⋯
CH_3CH_2	1586 ± 5[c]	441 ± 6	-12 ± 7	-185 ± 5	980 ± 15
CD_3CD_2	1582 ± 9[d]	436 ± 10	⋯	⋯	⋯
$(CH_3)_2CH$	1578 ± 3[e] (1576 ± 4[c])	445 ± 4	-46 ± 5	-231 ± 4	840 ± 10
$(CH_3)_3C$	1575 ± 3[e] (1573 ± 3[c])	447 ± 4	-83 ± 5	-274 ± 4	810 ± 10

[a]Reference 47.
[b]Reference 48.
[c]Reference 49.
[d]Reference 26.
[e]Reference 50.

EAs of $(CH_3)_2CHO$ and $(CH_3)_3CO$ is only half that amount. This indicates that the degree of perturbation of the system decreases when substituting the last H in CH_3O for a methyl group.

It is also interesting to note that the same decrease in EA, 0.013 eV, is observed upon deuteration for both CH_3O and CH_3CH_2O. This implies that deuteration decreases the zero point energy by a greater amount in the radical than in the anion.

The heat of formation of the cation also displays a stabilization effect with increasing size of R. It should be noted that $\Delta_f H_{300}(RO^+)$ is highly dependent on the value of $IP_0(RO)$, and in the case of $(CH_3)_2CHO$ and $(CH_3)_3CO$, the IP_0 values used are the only available measurements and have not been confirmed recently.

IV. CONCLUSION

Photoelectron spectra of alkoxides were presented and analyzed. Jahn-Teller effects dominate the CH_3O^- and CD_3O^- spectra, with peaks of contrasting β value carrying different vibronic symmetry assignments. The splitting between the ground $\tilde{X}\,^2A''$ and first excited $\tilde{A}\,^2A'$ states of CH_3CH_2O is observed directly at 355 ± 10 cm^{-1}. This close spacing causes vibronic coupling between the two states that perturbs vibrational levels; as a result, the ability of theoretical calculations to effectively explain the vibrational structure of CH_3CH_2O is hindered. Both the $(CH_3)_2CHO^-$ and $(CH_3)_3CO^-$ spectra show good agreement with theoretical predictions. The splitting between the ground $\tilde{X}\,^2A'$ and first excited $\tilde{A}\,^2A''$ states of $(CH_3)_2CHO$ is determined to be 1225 ± 65 cm^{-1}. No vibronic coupling is observed directly for $(CH_3)_2CHO$, as is true for Jahn-Teller activity in $(CH_3)_3CO$. There is no evidence of photodissociation of the species in any of the spectra. Finally, the electron affinities of all six neutrals (RO) were measured, showing good agreement with previous measurements, and in some cases to much greater accuracy. Values of D_{300}(RO–H), as well as the heat of formation for the alkoxide neutrals, anions, and cations are tabulated.

ACKNOWLEDGMENTS

This research is supported by the National Science Foundation. We would like to thank Dr. Friedrich Temps, Dr. Kent Ervin, and Dr. David Osborn for providing data prior to publication, Dr. Timothy Barckholtz for calculations on $(CH_3)_3CO$ and helpful discussions, and Dr. G. Barney Ellison also for helpful discussions.

[1] D. K. Russell and H. E. Radford, J. Chem. Phys. **72**, 2750 (1980).
[2] Y. Endo, S. Saito, and E. Hirota, J. Chem. Phys. **81**, 122 (1984).
[3] P. C. Engelking, G. B. Ellison, and W. C. Lineberger, J. Chem. Phys. **69**, 1826 (1978).
[4] H. R. Wendt and H. E. Hunziker, J. Chem. Phys. **71**, 5202 (1979).
[5] K. Ohbayashi, H. Akimoto, and I. Tanaka, J. Phys. Chem. **81**, 798 (1977).
[6] B. K. Janousek, A. H. Zimmerman, K. J. Reed, and J. I. Brauman, J. Am. Chem. Soc. **100**, 6142 (1978).
[7] G. Inoue, H. Akimoto, and M. Okuda, J. Chem. Phys. **72**, 1769 (1980).
[8] G. Inoue, H. Akimoto, and M. Okuda, Chem. Phys. Lett. **63**, 213 (1979).
[9] T. Ebata, H. Yanagishita, K. Obi, and I. Tanaka, Chem. Phys. **69**, 27 (1982).
[10] S. C. Foster, Y. Hsu, C. P. Damo, X. Liu, C. Kung, and T. A. Miller, J. Phys. Chem. **90**, 6766 (1986).
[11] S. C. Foster, P. Misra, T. D. Lin, C. P. Damo, C. C. Carter, and T. A. Miller, J. Phys. Chem. **92**, 5914 (1988).
[12] K. Fuke, K. Ozawa, and K. Kaya, Chem. Phys. Lett. **126**, 119 (1986).
[13] X. M. Liu, C. P. Damo, T. Lin, S. C. Foster, P. Misra, L. Yu, and T. A. Miller, J. Phys. Chem. **93**, 2266 (1989).
[14] P. Misra, X. Zhu, C. Hsueh, and J. Halpern, Chem. Phys. **178**, 377 (1993).
[15] S. D. Brossard, P. G. Carrick, E. L. Chappell, S. C. Hulegaard, and P. C. Engelking, J. Chem. Phys. **84**, 2459 (1986).
[16] Y.-Y. Lee, G. Wann, and Y.-P. Lee, J. Chem. Phys. **99**, 9465 (1993).
[17] D. E. Powers, M. B. Pushkarsky, and T. A. Miller, J. Chem. Phys. **106**, 6863 (1997).
[18] A. Geers, J. Kappert, F. Temps, and T. J. Sears, J. Chem. Phys. **98**, 4297 (1993).
[19] F. Temps (private communication).
[20] K. B. Wiberg, J. Am. Chem. Soc. **112**, 3379 (1990).
[21] D. R. Yarkony, H. F. Schaefer, III, and S. Rothenberg, J. Am. Chem. Soc. **96**, 656 (1974).
[22] G. D. Bent, G. F. Adams, R. H. Bartram, G. D. Purvis, and R. J. Bartlett, J. Chem. Phys. **76**, 4144 (1982).
[23] H. Koppel, Z. Phys. Chem. **200**, 3 (1997).
[24] T. A. Barckholtz and T. A. Miller, Int. Rev. Phys. Chem. **17**, 435 (1998).
[25] G. B. Ellison, P. C. Engelking, and W. C. Lineberger, J. Phys. Chem. **86**, 4873 (1982).
[26] T. T. Dang, E. L. Motell, M. J. Travers, E. P. Clifford, G. B. Ellison, C. H. DePuy, and V. M. Bierbaum, Int. J. Mass Spectrom. Ion Processes **123**, 171 (1993).
[27] S. C. Foster and T. A. Miller, J. Phys. Chem. **93**, 5986 (1989).
[28] G. Inoue, M. Okuda, and H. Akimoto, J. Chem. Phys. **75**, 2060 (1981).
[29] X. Q. Tan, J. M. Williamson, S. C. Foster, and T. A. Miller, J. Phys. Chem. **97**, 9311 (1993).
[30] X. Zhu, M. M. Kamal, and P. Misra, Pure Appl. Opt. **5**, 1021 (1996).
[31] L. A. Curtiss, D. J. Lucas, and J. A. Pople, J. Chem. Phys. **102**, 3292 (1995).
[32] C. Sosa and H. B. Schlegel, J. Am. Chem. Soc. **109**, 7007 (1987).
[33] R. J. Balla, H. H. Nelson, and J. R. McDonald, Chem. Phys. **99**, 323 (1985).
[34] (a) D. G. Leopold, K. K. Murray, A. E. Stevens-Miller, and W. C. Lineberger, J. Chem. Phys. **83**, 4849 (1985); (b) K. M. Ervin and W. C. Lineberger, *Photoelectron Spectra of Negative Ions* (JAI, Greenwich, 1992), Vol. 1.
[35] C. E. Moore, Atomic Energy Levels, U.S. GPO, Natl. Bur. Stand. (U.S.) Cir. 467 (1952).
[36] J. Cooper and R. Zare, J. Chem. Phys. **48**, 942 (1968).
[37] R. L. Schwartz, G. E. Davico, T. M. Ramond, and W. C. Lineberger, J. Phys. Chem. **103**, 8213 (1999).
[38] M. J. Frisch, G. W. Trucks, H. B. Schlegal, P. M. W. Gill, B. G. Johnson, M. A. Robb, J. R. Cheeseman, T. Kieth, G. A. Petersson, J. A. Montgomery, K. Raghavachari, M. A. Al-Laham, V. G. Zakrewski, J. V. Ortiz, J. B. Foresman, J. Cioslowski, B. B. Stefanov, A. Nanayakkara, M. Challacombe, C. Y. Peng, P. Y. Ayala, W. Chen, M. W. Wong, J. L. Andres, E. S. Replogle, R. Gomperts, R. L. Martin, D. J. Fox, J. S. Binkley, D. J. Defrees, J. Baker, J. P. Stewart, M. Head-Gordon, C. Gonzalez, and J. A. Pople, GAUSSIAN94, Revision E.1, Gaussian, Inc., Pittsburgh, Pennsylvania, 1995).
[39] We wish to thank Peter Chen and Cameron Logan for providing a copy of their CDECK program.
[40] D. L. Osborn, D. J. Leahy, E. H. Kim, E. deBeer, and D. M. Neumark, Chem. Phys. Lett. **292**, 651 (1998).
[41] K. M. Ervin and W. C. Lineberger, J. Phys. Chem. **95**, 1167 (1991).
[42] F. Temps, *Molecular Dynamics and Spectroscopy by Stimulated Emission Pumping* (World Scientific, Singapore, 1995).
[43] P. G. Carrick, S. D. Brossard, and P. C. Engelking, J. Chem. Phys. **83**, 1995 (1985).
[44] L. S. Alconcel, J. A. Davies, H. J. Deyerl, and R. E. Continetti (unpublished work).
[45] T. A. Barckholtz and T. A. Miller, J. Phys. Chem. **103**, 2321 (1999).
[46] T. A. Barckholtz (private communication).
[47] D. L. Osborn, D. J. Leahy, E. M. Ross, and D. M. Neumark, Chem. Phys. Lett. **235**, 651 (1995).

[48] M. J. Haas and A. G. Harrison, Int. J. Mass Spectrom. Ion Processes **124**, 115 (1993).
[49] V. F. deTuri and K. M. Ervin, J. Phys. Chem. **103**, 6911 (1999).
[50] S. G. Lias, J. E. Bartmess, J. F. Liebman, J. L. Holmes, R. D. Levin, and W. G. Mallard, J. Phys. Chem. Ref. Data **17**, Suppl. No. 1 (1988); K. M. Ervin, S. Gronert, S. E. Barlow, M. K. Gilles, A. G. Harrison, V. M. Bierbaum, C. H. DePuy, W. C. Lineberger, and G. B. Ellison, J. Am. Chem. Soc. **112**, 5750 (1990); D. H. Mordaunt and M. N. R. Ashfold, J. Chem. Phys. **101**, 2630 (1994); V. F. DeTuri, M. A. Su, and K. M. Ervin, J. Phys. Chem. **103**, 1468 (1999).
[51] G. B. Ellison, G. E. Davico, V. M. Bierbaum, and C. H. DePuy, Int. J. Mass Spectrom. Ion Processes **156**, 109 (1996).
[52] C. E. Moore, *Atomic Energy Levels* (National Bureau of Standards, Washington, D.C., 1971).
[53] J. B. Pedley, R. D. Naylor, and S. P. Kirby, *Thermochemical Data of Organic Compounds* (Chapman and Hall, New York, 1986).
[54] B. Ruscic and J. Berkowitz, J. Chem. Phys. **95**, 4033 (1991).
[55] B. Ruscic and J. Berkowitz, J. Chem. Phys. **101**, 10 936 (1994).
[56] J. M. Williams and W. H. Hamill, J. Chem. Phys. **49**, 4467 (1968).